A Multispectral Thermometry Based on the Self-adaptive Cuckoo Algorithm

Zemeng Yang¹, Yucun Zhang^{1,*}, Tao Kong²

¹School of Electrical Engineering, Yanshan University, HaiGang Distinct, HEBEI Street, Qinhuangdao City 066000, Hebei Province, China

²Hebei University of Environment Engineering, Beidaihe Distinct, Jingang Avenue, Qinhuangdao City 066102, Hebei Province, China

*Corresponding author.

Abstract

Multispectral thermometry stands as a prevalent non-contact method utilized for temperature measurement across various applications. To solve the problem that multispectral thermometry cannot obtain accurate temperature of the target under the unknown spectral emissivity, many scholars have proposed various optimization algorithms. However, there are still problems such as the large emissivity search range, uncertain initial solution and long solution time. To solve the above problems, a new objective function and constraint conditions are established. A self-adaptive cuckoo algorithm is proposed. Real number coding is used to improve the convergence ability and robustness of the algorithm. The adaptive function is used to evaluate the quality of the solution, and the result is avoided to fall into the local optimal solution by the random walk mechanism of Lévy flight. The validity of the proposed self-adaptive cuckoo algorithm is verified by inversion calculation of 6 different emissivity models and zirconia samples. The maximum relative error of self-adaptive cuckoo algorithm is 0.41% in the case of no noise interference, and 0.91% in the case of noise interference. The selfadaptive cuckoo algorithm can still inversion the temperature well with a low signal-tonoise ratio. The experimental results show that the inversion temperature error is less than 0.25%. This method provides a new idea for multispectral temperature measurement.

Keywords: Multispectral thermometry, Constrained optimization, Self-adaptive cuckoo algorithm, Emissivity.

1. Introduction

Multispectral thermometry is a used and effective non-contact method of temperature measurement [1-2]. The multispectral thermometry is suitable for the simultaneous measurement of temperature and material emissivity. It has the advantages of no special requirements for the measured object, high temperature measurement accuracy, fast response time and simple component [3-5]. By leveraging multiple spectral bands, this method offers enhanced accuracy for diverse materials and scenarios, making it an indispensable tool in various industrial and scientific applications, ranging from material analysis to industrial process monitoring and control.

Multispectral thermometry has made great progress in true temperature measurement and target emissivity calculations ^[6-8]. Traditional multispectral thermometry solves the temperature solution under unknown spectral emissivity by establishing a wavelength-emissivity model or a temperature-emissivity model ^[9-11]. But the emissivity model is only applicable to the specific material, and the measurement accuracy can be guaranteed when the model is consistent with the actual situation ^[12-13]. While effective, these traditional methods are

International Journal of Multiphysics Volume 18, No. 3, 2024

ISSN: 1750-9548

constrained by their material specificity and the requisite assumptions for accurate measurements. Novel advancements have emerged to address these limitations, aiming to offer more generalized and adaptable solutions for temperature measurement and emissivity determination across various materials and scenarios. The development of such methods broadens the applicability of multispectral thermometry, allowing for more precise and reliable temperature measurements independent of material-specific assumptions. These breakthroughs signify a significant shift in the field, paving the way for enhanced accuracy and broader real-world applicability in temperature measurement and emissivity calculations.

In recent years, significant advancements have been made in the field of multispectral thermometry, particularly in the development of non-contact temperature measurement models that do not rely on emissivity assumptions. Researchers have turned to constrained optimization algorithms to address the challenges associated with traditional methods. The exploration of these innovative approaches has led to noteworthy developments aimed at enhancing accuracy, computational efficiency, and real-time applicability. The introduction of optimization methods within multispectral thermometry gained notable attention in 2006 when Dai pioneered the integration of the genetic algorithm for optimizing reference temperature mathematical models in the measurement of rocket plume temperature^[14]. Although this approach demonstrated promise, there were notable limitations concerning inversion accuracy and computational speed. Subsequent efforts brought forward improved techniques, emphasizing the elimination of emissivity constraints. In 2017, Jian introduced a generalized inverse matrix-external penalty function algorithm without requiring object emissivity information^[15]. This approach significantly boosted computational efficiency and achieved a calculating speed nearly in real-time. Building upon this, Liang further refined the generalized inverse matrix-external penalty function algorithm in 2018^[16]. This newer method utilized a set of emissivity values obtained through the generalized inverse matrix technique as the initial basis for an iterative algorithm. As a result, it became possible to simultaneously retrieve emissivity and true temperature. Notably, while this advancement enhanced the accuracy of the inversion temperature solution, it still depended on approximate emission ranges rooted in prior knowledge, presenting challenges in obtaining exact emissivity values in practical applications. Subsequently, Zhang proposed a multispectral thermometry approach based on multi-objective constrained optimization in 2022^[17]. This method enables the precise determination of true temperature and spectral emissivity without the need for prior emissivity information. Despite the advantage of not relying on an emissivity assumption model, this new approach necessitates the narrowing of the emissivity search range and the identification of a suitable initial solution. Challenges persist as the calculation time sometimes falls short of meeting real-time requirements, and maintaining high accuracy in temperature calculation is problematic. Furthermore, the optimization algorithm faces the issue of multiple local minima in the objective function. Through these developments, it is evident that while significant strides have been made toward temperature and emissivity retrieval, practical challenges remain. Enhancing the speed and accuracy of these calculations while maintaining real-time capabilities is a critical ongoing objective within this domain. As research progresses, addressing these intricacies will likely pave the way for more robust and efficient methods in thermal analysis. When the optimization result of the function is the local minimum, there will still produce large error in the calculating. Therefore, even if the optimal result of the function is valid, the calculation result of the temperature may be invalid.

Based on the aforementioned scenario, an enhanced and expanded data processing model for multispectral thermometry has been devised, taking into account the interplay between the calculated temperatures from three adjoining channels, the deviation from actual temperatures, and the complex relationships between emissivity, detection signal, and reference signal. Through this comprehensive reassessment, the objective function and constraint conditions have been redefined, laying the groundwork for the establishment of a new data processing model in multispectral thermometry. Thus, a new data processing model of multispectral thermometry is established. A self-adaptive cuckoo algorithm(SACS) is proposed. Real number coding is used to improve the convergence ability and robustness. The adaptive function is used to evaluate the quality of the solution, and the result is avoided to fall into the local optimal solution by the random walk mechanism of Lévy flight. The validity of the proposed self-adaptive cuckoo algorithm is verified by inversion calculation of 6 different emissivity models and zirconia samples.

2. Theoretical Research

According to the multispectral thermometry theory, the reference temperature model can be obtained [18]

$$\frac{V_i}{V_i'} = \varepsilon \left(\lambda_i, T\right) e^{\frac{C_2}{\lambda_i} \left(\frac{1}{T'} - \frac{1}{T}\right)} \tag{1}$$

where T represents the true temperature of the target object. T' signifies the black body reference temperature. V_i and V_i ' stand for the output signals of the ith channel at temperature T and T', respectively. C_2 denotes the second radiation constant, holding a value of $1.4388 \times 104 \ \mu \text{m·K}$. λ_i represents the effective wavelength of the ith spectral channel, and $\varepsilon(A_{\lambda i}, T)$ corresponds to the emissivity of the target object at wavelength λ_i and temperature T.

Eq. (1) cannot be solved because of two unknown quantities. Consequently, an emissivity hypothetical model is devised for temperature inversion calculation. Nevertheless, the congruence between the assumed model and true emissivity markedly impacts temperature measurement accuracy. Substantial deviations between the assumed model and actual emissivity result in considerable errors in temperature and emissivity calculations. To address this issue, a novel approach has been introduced. This new method aims to mitigate the impact of assumed emissivity models on temperature measurement accuracy. Through this innovation, the goal is to improve the precision of temperature and emissivity calculations by minimizing errors stemming from discrepancies between assumed and actual emissivity values. The existing predicament outlined by Eq. (1) highlights the interdependence of temperature calculation and emissivity determination. The proposed approach seeks to establish a more robust and adaptable methodology to better accommodate deviations between assumed and actual emissivity, ultimately enhancing the accuracy of temperature measurements. By systematically addressing the impact of emissivity deviation on temperature calculation, this method aims to offer an effective solution that minimizes errors associated with assumed emissivity models. Through this novel approach, the intention is to significantly improve the reliability and precision of temperature measurements in scenarios where accurate emissivity values are challenging to ascertain.

Taking the logarithm on the Eq. (1)

$$\ln\left(\frac{V_i}{V_i'}\right) - \frac{C_2}{\lambda_i T'} = -\frac{C_2}{\lambda_i T} + \ln \varepsilon \left(\lambda_i, T\right)$$
(2)

The true temperature *T* is calculated as

$$T_{i} = \frac{1}{\frac{1}{T'} + \frac{\lambda_{i}}{C_{2}} \left[\ln \varepsilon \left(\lambda_{i}, T \right) - \ln \left(\frac{V_{i}}{V_{i}'} \right) \right]}$$
(3)

Theoretically, the calculated temperature of each spectral channel is the same ($T_1=T_2=...=T_n$), and the following relationship exists between the three adjacent channels

$$\frac{TT_{i+2}}{T_{i+1}} = T \tag{4}$$

Owing to uncertain emissivity and random measurement errors, temperatures vary across channels. This inconsistency aligns with error theory:

$$\min F = \left[\sum_{i=1}^{n-2} \left(\frac{T_i T_{i+2}}{T_{i+1}} \right) - E(T_i) \right]^2 \to 0$$
 (5)

where $E(T_i)$ is the average calculated temperature of each spectral channel, which can be expressed as

ISSN: 1750-9548

$$E(T_i) = \frac{1}{n} \sum_{i=1}^{n} T_i \tag{6}$$

Therefore, the objective function F is established as

$$\min F = \left[\sum_{i=1}^{n-2} \left(\frac{T_i T_{i+2}}{T_{i+1}} \right) - E(T_i) \right]^2$$
 (7)

Since the temperature of each spectral channel is theoretically calculated to be equal $(T_i=T_{i+1})$, meaning that $\frac{1}{T_i}=\frac{1}{T_{i+1}}$. Substituting Eq. (3) to

$$\lambda_{i} \left[\ln \varepsilon \left(\lambda_{i}, T \right) - \ln \left(\frac{V_{i}}{V_{i}'} \right) \right] = \lambda_{i+1} \left[\ln \varepsilon \left(\lambda_{i+1}, T \right) - \ln \left(\frac{V_{i+1}}{V_{i+1}'} \right) \right]$$
(8)

When $0 < \lambda_i < \lambda_{i+1}$, the inequality can be obtained from Eq. (8)

$$0 < \frac{\ln\left[\frac{\varepsilon(\lambda_{i+1}, T)V'_{i+1}}{V_{i+1}}\right]}{\ln\left[\frac{\varepsilon(\lambda_{i}, T)V'_{i}}{V_{i}}\right]} < 1$$
(9)

According to the Eq. (9), the constraints are discussed and be obtained:

$$\begin{cases}
\frac{\varepsilon(\lambda_{i},T)V_{i}'}{V_{i}} - \frac{\varepsilon(\lambda_{i+1},T)V_{i+1}'}{V_{i+1}} > 0, & \text{when } \varepsilon(\lambda_{i},T)V_{i}' > V_{i} \\
\frac{\varepsilon(\lambda_{i+1},T)V_{i+1}'}{V_{i+1}} - \frac{\varepsilon(\lambda_{i},T)V_{i}'}{V_{i}} > 0, & \text{when } 0 < \varepsilon(\lambda_{i},T)V_{i}' < V_{i}
\end{cases}$$
(10)

Combining with the objective function in Eq. (7), the multispectral thermometry problem is transformed into a constrained optimization problem:

$$\begin{aligned}
&\min F = \left[\sum_{i=1}^{n-2} \left(\frac{T_{i}T_{i+2}}{T_{i+1}}\right) - E\left(T_{i}\right)\right]^{2} \\
&\frac{\varepsilon\left(\lambda_{i}, T\right)V_{i}'}{V_{i}} - \frac{\varepsilon\left(\lambda_{i+1}, T\right)V_{i+1}'}{V_{i+1}} > 0, & \text{when } \varepsilon\left(\lambda_{i}, T\right)V_{i}' > V_{i} \\
&\frac{\varepsilon\left(\lambda_{i+1}, T\right)V_{i+1}'}{V_{i+1}} - \frac{\varepsilon\left(\lambda_{i}, T\right)V_{i}'}{V_{i}} > 0, & \text{when } 0 < \varepsilon\left(\lambda_{i}, T\right)V_{i}' < V_{i}
\end{aligned}$$
(11)

3. Self-adaptive Cuckoo Algorithm

The cuckoo algorithm (CS) is derived from the reproductive behavior of the cuckoo. The process of the cuckoo finding a nest successfully is called optimization. In the CS algorithm, each nest corresponds to a feasible solution, and the new or potential solution is used to replace the poorer solution. The CS algorithm has small parameters, easy operation, simple model and strong global search ability. However, the search process of the traditional CS algorithm completely depends on the random wandering mechanism of the Lévy flight, which has too much randomness. Therefore, CS algorithm has many problems, such as large randomness, low algorithm search efficiency, poor accuracy of the later search and slow convergence speed.

Based on the above situation, a self-adaptive cuckoo algorithm(SACS) is proposed. Real number coding is used to improve the convergence ability and robustness of the CS algorithm. The SACS algorithm generates new solutions by variation and cross operation. And the feasible solution is obtained in the solution space quickly by using an adaptation function to evaluate the quality of the solutions. And the result is avoided to fall into the local optimal solution by the random walk mechanism of Lévy flight. The SACS algorithm's refinement not

only rectifies the limitations of the traditional CS approach but also introduces a more controlled and adaptive search process, thereby enhancing overall algorithmic performance. By mitigating the excessive randomness and improving search efficiency, the SACS algorithm offers a more balanced and effective approach to optimization tasks, fostering increased accuracy, faster convergence, and greater adaptability across diverse problem domains. Overall, the introduction of the SACS algorithm represents a significant step forward in enhancing the efficacy and reliability of cuckoo-inspired optimization techniques.

The Lévy flight can be described as a moving entity moves in a relatively small step, it suddenly takes a large step in a random direction. The movement step size is distributed according to the power law. This method makes the step size very random and can search the optimal solution over a wider space. The global random wander formula of CS algorithm based on Lévy flight is:

$$X_i^{t+1} = X_i^t + \alpha \otimes L\acute{e}vy(\beta) \tag{12}$$

Where X_i^t denotes the position of the *i*th nest in generation t, α stands for the step size multiplier, and Lévy(β) is the Lévy flight random search path, as well as its moving step follows Lévy probability distribution:

$$L\acute{e}vy(\beta) \square \mu = t^{-\lambda}, 1 \le \beta \le 3$$
 (13)

The SACS algorithm avoids fall into the local optimal solution by Lévy flight, and obtains the optimal solution by the selection operation. The main steps of the DECS algorithm are:

Step 1: Set relevant parameters and initialize the population. The population size is N_p , the individuals in the population are denoted as $x_i=(d_{i,1}, d_{i,2}, d_{i,k}, ..., d_{i,D})$, and the fitness is calculated.

Step 2: The variation vector $v_i^{g+1} = x_{r_1}^g + B(x_{r_2}^g - x_{r_3}^g)$ ($i \neq r_1 \neq r_2 \neq r_3$) affecting the next generation is generated under the action of difference variation operator containing variation factor B, and x_i^g denotes the ith individual in the gth generation.

Step 3: An individual-to-individual cross operation is carried out between the gth generation population x_i^g and

its variant intermediate v_i^{g+1} , that is $u_{j,i}^{g+1} = \begin{cases} v_{j,i}^{g+1}, & \text{if } rand(0,1) \leq CR \text{ or } j = j_{rand} \\ x_{j,i}^g, & \text{otherwise} \end{cases}$. Where CR is the crossover

probability, and j_{rand} is any integer between [1,2,...,D].

Step 4: Using the greedy algorithm $x_i^{g+l} = \begin{cases} u_i^{g+l}, & \text{if } f\left(u_i^{g+l}\right) \leq f\left(x_i^g\right) \\ x_i^g, & \text{otherwise} \end{cases}$ to perform the selection operation. Where x_i^g

is the population of the previous generation, and u_i^g is the population after the crossover. The objective function value of the new solution vector is calculated. If the new solution vector has a better objective function value, the original solution vector is replaced, otherwise, the original solution vector will not be replaced.

Step 5: Continue with Step 2 iteratively until convergence or until the maximum number of iterations is attained.

Step 6: The optimal solution vector in the population and several adjacent solution vectors are selected as the initial location of the new population and nest.

Step 7: Update the contemporary nest position according to Lévy flight: $P_{t-1} = \left[X_1^{t-1}, X_2^{t-1}, \dots, X_n^{t-1}\right]^T$. Replace the poor adapted nest position with the good adapted nest position, and the contemporary nest position is defined as: $g_t = \left[X_1^t, X_2^t, \dots, X_n^{t-1}\right]$.

Step 8: A random number R is used as the probability that the owner of the nest will find the alien egg. And compared R with the finding probability $P_a(P_a \in [0,1])$. If $R > P_a$, the nest position in gt will be randomly changed. If $R \le P_a$, the nest position in g_t remains the same. Update the nest locations to obtain a better set of

ISSN: 1750-9548

nest locations: $P_t = [X_1^t, X_2^t, ..., X_n^t]^T$. Therefore, update the optimal nest location X_{best}^t and the optimal solution f_{\min}^t .

Step 9: Check whether the algorithm meets the maximum number of iterations. If not, repeat Step 7.

Step 10: End the search process and output the global optimal solution fmin.

4. Simulation Analysis

Let $\frac{V_i'}{V_i} = a_i$, $\varepsilon(\lambda_i, T) = x_i$, and convert the constraint into the linear inequality $Ax \ge b$:

$$\begin{cases}
 a_{1}x_{1} - a_{2}x_{2} > 0 \\
 a_{2}x_{2} - a_{3}x_{3} > 0 \\
 \vdots \\
 a_{n-1}x_{n-1} - a_{n}x_{n} > 0
\end{cases}$$

$$\begin{vmatrix}
 -a_{1}x_{1} + a_{2}x_{2} > 0 \\
 -a_{2}x_{2} + a_{3}x_{3} > 0 \\
 \vdots \\
 -a_{n-1}x_{n-1} + a_{n}x_{n} > 0$$
(14)

Let

$$A = \begin{bmatrix} a_1 & -a_2 & 0 & \cdots & 0 & 0 \\ 0 & a_2 & -a_3 & \cdots & 0 & 0 \\ \vdots & \vdots & \vdots & \ddots & \vdots & \vdots \\ 0 & 0 & 0 & \cdots & a_{n-1} & -a_n \end{bmatrix} \begin{bmatrix} -a_1 & a_2 & 0 & \cdots & 0 & 0 \\ 0 & -a_2 & a_3 & \cdots & 0 & 0 \\ \vdots & \vdots & \vdots & \ddots & \vdots & \vdots \\ 0 & 0 & 0 & \cdots & -a_{n-1} & a_n \end{bmatrix}$$
(15)

$$x = \begin{bmatrix} \varepsilon_1 & \varepsilon_2 & \cdots & \varepsilon_n \end{bmatrix}^T \text{ or } \begin{bmatrix} \varepsilon_1 & \varepsilon_2 & \cdots & \varepsilon_n \end{bmatrix}^T$$
 (16)

$$b = \begin{bmatrix} 0 & 0 & \cdots & 0 \end{bmatrix}_n^T \begin{bmatrix} 0 & 0 & \cdots & 0 \end{bmatrix}_n^T$$
 (17)

Employing the Lagrange multiplier method helps transform the constrained optimization problem into an unconstrained optimization problem. Thereby, facilitating a more tractable mathematical formulation. Through this approach, the Lagrange function is constructed, enabling the incorporation of constraints into the optimization process, resulting in a unified objective function. This methodology not only simplifies the optimization process but also allows for the efficient exploration of the solution space while accommodating the requisite constraints.

$$\begin{cases}
L(x, r^{2}) = F + \sum_{i=1}^{n-1} r_{i}^{1} h_{i}(x), & \text{when } \varepsilon(\lambda_{i}, T) V_{i}' > V_{i} \\
L(x, r^{1}) = F + \sum_{i=1}^{n-1} r_{i}^{2} h_{i}(x), & \text{when } 0 < \varepsilon(\lambda_{i}, T) V_{i}' < V_{i}
\end{cases}$$
(18)

Where F is the objective function established, $h_i(x) = A_i x_i - b_i$, Ai is the ith row element of the constraint matrix coefficient A, and b_i is the ith row vector of the constraint matrix vector b.

When the optimal solution x^* of the objective function is located in the feasible domain, the Lagrange function needs to satisfy

$$\begin{cases} h(x^*) > 0 \\ \nabla_x f(x^*) = 0 \\ \nabla_{xx} f(x^*) \text{ is a positive semi-definite matrix} \end{cases}$$
 (19)

When the optimal solution x^* of the objective function lies outside the feasible domain, the Lagrange function needs to satisfy

$$\begin{cases} h(x^*) = 0 \\ \nabla_x f(x^*) = r \nabla_x h(x^*) \\ y' \nabla_{xx} L(x^*) y \ge 0 \end{cases}$$
 (20)

In summary, the Lagrange function needs to satisfy

$$\begin{cases} \nabla_{x}L(x^{*}, r^{*}) = 0 \\ r^{*} \leq 0 \\ r^{*}h(x^{*}) = 0 \end{cases}$$

$$h(x^{*}) \geq 0$$
Plus positive definite constraints on $\nabla_{x}L(x^{*}, r^{*})$

Based on the objective function and constraints established above, six target materials labelled as A-F with different emissivity trends were simulated by using SACS algorithm. By leveraging the SACS algorithm in this context, it becomes possible to accurately capture and analyze the emissivity behavior of the selected materials under specific temperature conditions, thereby providing crucial insights into their thermal properties. The emissivity models of the six target materials at different wavelengths with the temperature is 1200 K are shown in Table 1.

Target 0.7 µm 0.9 µm 1.1 μ<u>m</u> $0.4~\mu m$ 0.5 µm $0.6 \, \mu m$ $0.8~\mu m$ 1.0 µm 0.85 0.75 0.60 0.55 0.50 0.45 Α 0.67 0.48 В 0.45 0.48 0.50 0.55 0.60 0.67 0.75 0.85 C 0.45 0.55 0.65 0.75 0.74 0.65 0.55 0.45 D 0.85 0.75 0.65 0.55 0.54 0.65 0.75 0.80 Е 0.85 0.65 0.55 0.65 0.84 0.65 0.55 0.50 F 0.84 0.50 0.55 0.65 0.65 0.55 0.65 0.85

Table 1 Target Emissivity Model

The blackbody's reference temperature, set at 1500 K, is a crucial factor for precise thermal measurements. To ensure both computational efficiency and accuracy in inversion results, the multispectral pyrometer should be configured with 8 effective spectral channels. These channels, denoted as λ_1 - λ_8 , correspond to wavelengths of 0.4 µm- 1.1 µm. Configuring the multispectral pyrometer with these predetermined spectral channels allows for the acquisition of thermal radiation data across distinct wavelength ranges, thereby facilitating comprehensive spectral analysis. By capturing thermal emissions at these specific wavelengths, the multispectral pyrometer enables the assessment of material properties and temperature distribution with precision and accuracy. This strategic selection of spectral channels not only optimizes computational resources but also enhances the effectiveness of the thermal measurement process, offering valuable insights for diverse applications in fields such as material sciences, industrial processes, and environmental monitoring. Overall, the careful determination and utilization of these eight spectral channels within the multispectral pyrometer contribute significantly to the robustness and reliability of temperature inversion procedures, ultimately advancing the understanding and utilization of thermal data for a broad spectrum of scientific and industrial endeavors.

Optimize the data processing model in Eq. (11) according to the steps shown in Figure 1.

Table 2 shows the average inversion temperature, average absolute error and average relative error obtained by inversion of six materials using SACS algorithm.

Table 2 shows the SACS algorithm meter has a high accuracy of temperature inversion results for all six materials. Material E has the highest inversion temperature accuracy with the average absolute error is 0.05K and the average relative error is 0.01%. Material C has the highest inversion temperature error, however, the average absolute error is only 4.8K and the average relative error is only 0.41%. These results underline the algorithm's precision in deriving temperature data, solidifying its practical application in diverse production

ISSN: 1750-9548

settings. The temperature calculations produced by the SACS algorithm not only exhibit impressive accuracy but also establish their reliability for practical use. The temperature calculated by SACS algorithm is accurate and can be used in practical production. In addition, the calculation time of SACS algorithm is about 0.34s, which can be used as a method for processing multispectral thermometry (simulation environment: Matlab R2021b; 11th Gen Intel Core i5-11400 @ 2.60GHz; 8G RAM). These findings collectively emphasize the SACS algorithm's role as a robust and dependable tool for temperature inversion, offering a valuable resource for industries reliant on precise thermal measurements. Its exceptional accuracy and computational speed not only demonstrate its applicability across various material science and industrial domains but also underscore its potential to streamline and enhance thermal analysis processes, ultimately contributing to advancements in production, research, and technological innovation.

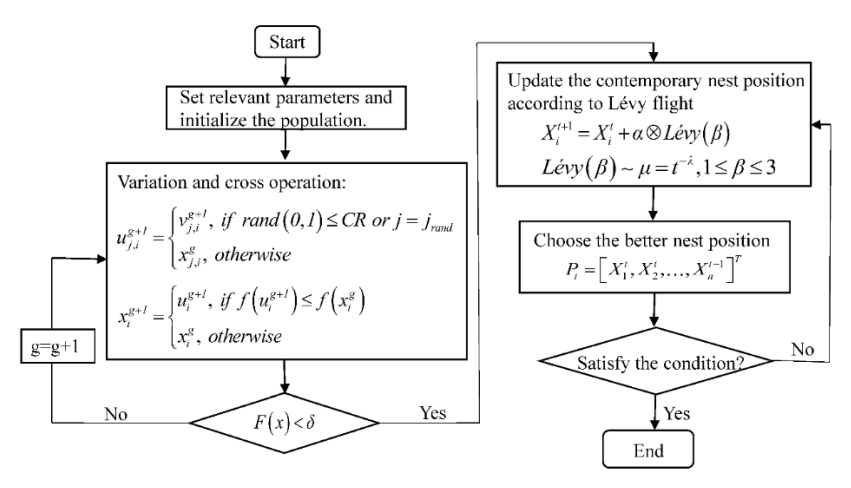


Figure 1 Program flow chart of the SACS algorithm

Table 2 Inversion of temperature results by SACS algorithm.

T=1200 K	A	В	С	D	Е	F
Average inversion temperature (K)	1199.38	1196.40	1195.20	1201.69	1199.95	1197.26
Average absolute error (K)	0.63	3.6	4.8	1.69	0.05	2.76
Average relative error (%)	0.05	0.31	0.41	0.14	0.01	0.22

Figure 2(a)-(f) depict the emissivity inversion results for six materials labeled A, B, C, D, E, and F, respectively. Fig. 2 shows that the emissivity inversion accuracy of the six materials is high, and the error between the calculated emissivity value and the true value of each channel is less than 0.1. These images effectively illustrate the high accuracy achieved in the emissivity inversion process for each material. Notably, the calculated emissivity values closely approximate the true values for each spectral channel, demonstrating an error margin of less than 0.1. The maximum absolute error in emissivity for material A, B, C, D, E and F are 0.01, 0.04, 0.09, 0.03, 0.01 and 0.04, respectively. These results not only underscore the accuracy of the emissivity inversion process but also align with the trends observed in the temperature inversion, further validating the robustness and reliability of the SACS algorithm. This is consistent with the results obtained from temperature inversion. The trend of emissivity variation with wavelength calculated by SACS algorithm is consistent with the true distribution. It is shown that the SACS algorithm can be used for spectral emissivity inversion. The findings portrayed in Figures 2(a)-(f) as well as the derived error metrics serve to reinforce the SACS algorithm's proficiency in capturing and analyzing emissivity data across various materials. This not only solidifies its utility within the domain of thermal analysis but also positions it as a pivotal tool for material characterization and assessment. Consequently, these results contribute to the broader understanding of spectral emissivity behavior, offering invaluable insights for fields such as material sciences, industrial processes, and environmental monitoring.

To investigate the stability of the SACS algorithm, the voltage signal in Eq.(1) is simulated by adding 1%, 10%, 20% and 40% of random noise. Table 3 shows the average inversion temperature, average absolute error and average relative error of the six materials inversion obtained by the SACS algorithm after adding different random noise. The deliberate introduction of incremental levels of random noise serves to evaluate the algorithm's resilience and performance under conditions of signal variability. By systematically testing the algorithm's response to increasing noise levels, the study seeks to provide insights into its ability to maintain accuracy and consistency in temperature inversion across different simulated signal distortions. Through this rigorous assessment, the study aims to ascertain the algorithm's reliability and robustness in delivering precise and consistent results, even in the presence of signal perturbations representative of real-world measurement scenarios. The comprehensive analysis of the algorithm's performance under varied noise conditions not only serves to validate its stability but also offers critical insights into its operational limits and potential improvements, thereby contributing to the ongoing refinement and optimization of the SACS algorithm for real-world applications across diverse industrial and scientific domains. This systematic evaluation establishes a significant foundation for understanding the algorithm's adaptability and its potential role in addressing challenges related to signal variability in practical multispectral thermometry applications.

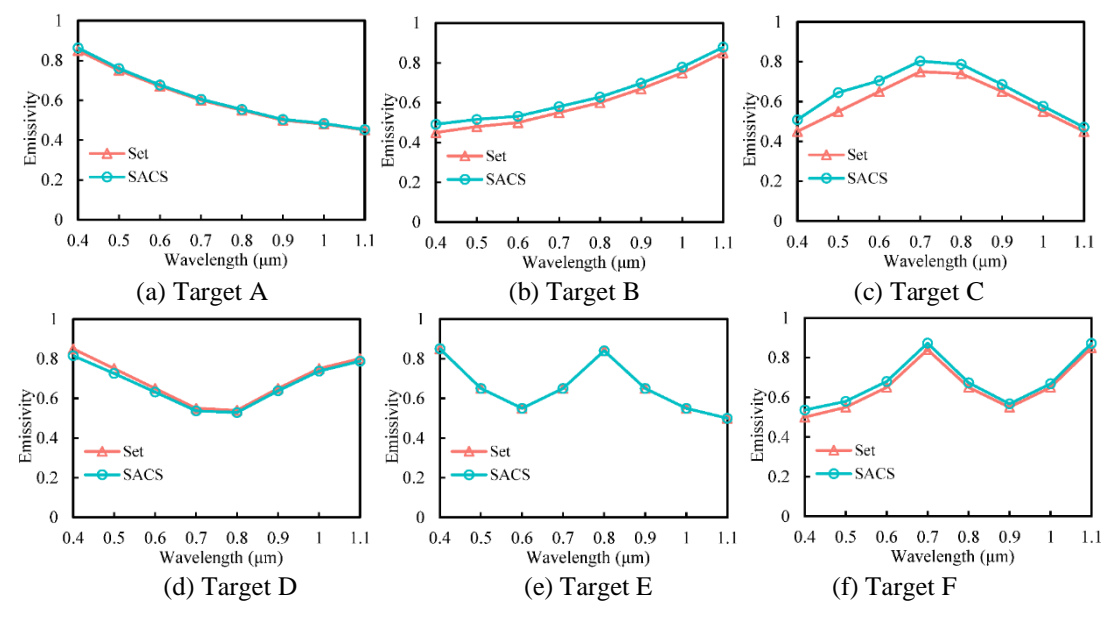


Figure 2 Emissivity inversion results of different materials

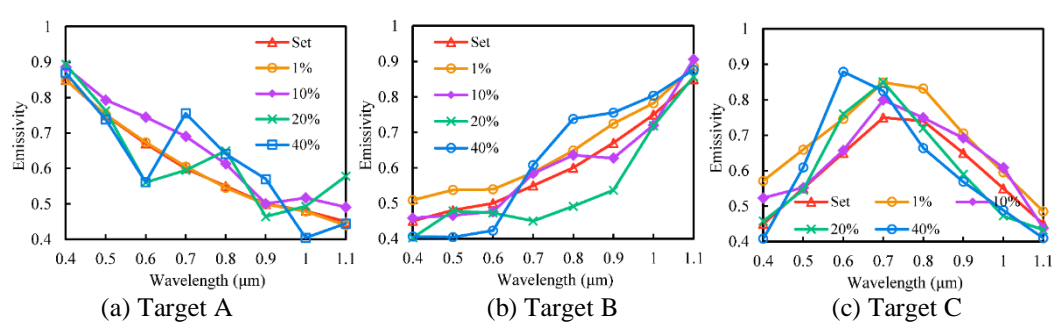
Table 3 Temperature simulation results of the SACS algorithm after adding different random noise.

	T=1200 K	A	В	С	D	Е	F
1% random noise	Average inversion temperature (K)	1200.35	1195.94	1191.50	1199.08	1197.14	1196.63
	Average absolute error (K)	0.35	5.19	8.50	0.92	2.86	3.37
	Average relative error (%)	0.03	0.34	0.71	0.08	0.24	0.28
10%	Average inversion temperature (K)	1194.25	1199.76	1196.87	1199.84	1197.40	1201.08
random noise	Average absolute error (K)	5.75	0.24	3.13	0.16	2.60	1.08
	Average relative error (%)	0.51	0.02	0.26	0.02	0.22	0.09
20% random	Average inversion temperature (K)	1196.58	1207.79	1199.01	1202.95	1210.93	1200.46

noise	Average absolute error (K)	3.42	7.79	0.99	2.95	10.93	0.46
	Average relative error (%)	0.29	0.65	0.08	0.25	0.91	0.04
40%	Average inversion temperature (K)	1198.75	1200.98	1202.20	1197.26	1194.96	1199.86
random	Average absolute error (K)	1.25	0.98	2.20	2.74	5.04	0.14
noise	Average relative error (%)	0.10	0.08	0.18	0.23	0.42	0.01

Table 3 shows that the temperature inversion error of C and F are the largest when the random noise is 1%, and the average absolute error is 8.5 K and 3.37 K, the average relative error is 0.71% and 0.28%, respectively. The temperature inversion error of material A is the largest when the random noise is 10%, and the average absolute error is 5.75K, the average relative error is 0.51%. The temperature inversion error of B, D and E are the largest when the random noise is 20%, and the average absolute error is 7.79 K, 2.95 K and 10.93 K, the average relative error is 0.65%, 0.25% and 0.91%, respectively. The SACS algorithm demonstrates minimal inversion temperature errors under random noise, showcasing high accuracy. Even under low signal-to-noise ratios, the SACS algorithm consistently produces reliable inversion results.

Figure 3(a)-(f) shows the emissivity inversion results of materials A, B, C, D, E and F under different random noise respectively. This comprehensive analysis demonstrates the algorithm's resilience in the presence of noise, showcasing its ability to maintain accuracy across different noise levels. Fig. 3 shows that when the random noise is 1% and 10%, the trend of the calculated emissivity with wavelength for the six materials are general agreement with the true distribution. When the random noise is 20%, the trend of the calculated emissivity with wavelength for materials C and E is generally consistent with the true distribution, while the trend of the calculated emissivity with wavelength for materials A, B, D and F is somewhat different from the true distribution. When the random noise is 40%, the simulation results are affected by interference. However, the trend of the emissivity variation with wavelength obtained from the simulation for the six materials can still fit with the true distribution. These observations collectively underscore the SACS algorithm's robustness in the face of interference, highlighting its adeptness in preserving accuracy under challenging conditions, particularly low signal-to-noise ratios. This resilience solidifies its suitability as a dependable method for temperature inversion and data processing in the realm of multispectral thermometry. The algorithm's capability to withstand noise and interference positions it as a vital tool for practical applications where such environmental factors are prevalent. Therefore, the SACS algorithm has strong anti-interference ability and can still perform temperature inversion well under the condition of low signal-to-noise ratio. It can be used as a data processing method for multispectral thermometry. Furthermore, these findings not only emphasize the algorithm's adaptability but also its potential to enhance data processing methodologies for thermal analysis. By withstanding varying degrees of noise and interference, the SACS algorithm emerges as an indispensable asset for industries reliant on precise thermal measurements, thereby contributing to advancements in material science, industrial processes, and environmental monitoring. In essence, the SACS algorithm's demonstrated resilience underscores its capacity to navigate real-world conditions, reinforcing its practical utility in effectively and accurately performing temperature inversion, thereby fortifying its status as a pivotal tool in multispectral thermometry.



ISSN: 1750-9548

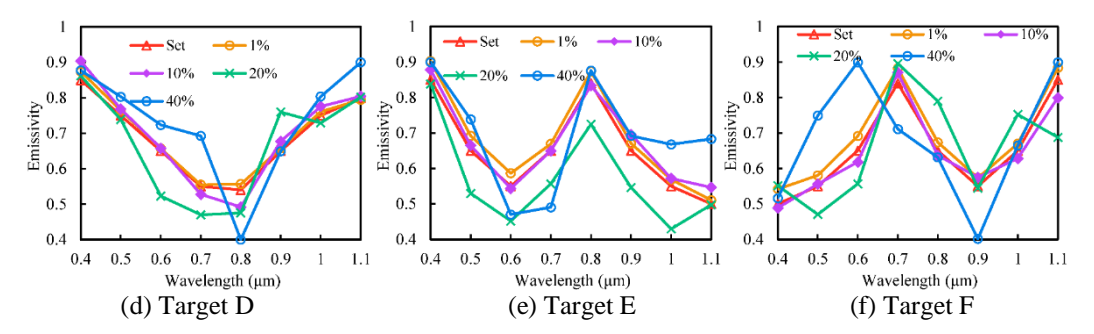


Figure 3. Emissivity inversion results of different materials with different random noises.

5. Experimental Verification

Experiment was established to verify the effectiveness of the proposed SACS algorithm. The data came from Kun ^[19]. The radiation signal of zirconia samples at 734K, 837K and 913K temperature were measured using a fourier spectrometer. The reference temperature of the blackbody is 653K. Table 4 displays the variance between the inversion temperature and the actual temperature, while the correspondence between the retrieved emissivity and the true emissivity is depicted in Fig. 4. This comparative illustration serves to underscore the algorithm's ability to discern and approximate the emissivity of zirconia samples across different temperature ranges, thereby highlighting its efficacy in capturing material-specific thermal responses. By employing this experimental approach, the study not only validates the SACS algorithm's performance but also contributes to the expanding body of evidence supporting its reliability in temperature inversion and emissivity retrieval. Such affirmative findings are integral in reinforcing the algorithm's utility in practical applications spanning material characterization, industrial processes, and thermal analysis, thereby positioning it as a pivotal tool in advancing our understanding of thermal behaviors and responses across various materials and temperature ranges.

Table 4 Temperature simulation results of the SACS algorithm under different true temperatures.

True temperature (K)	734	837	913
Average inversion temperature (K)	733.68	835.26	910.83
Average absolute error (K)	0.32	1.70	2.16
Average relative error (%)	0.04	0.20	0.24

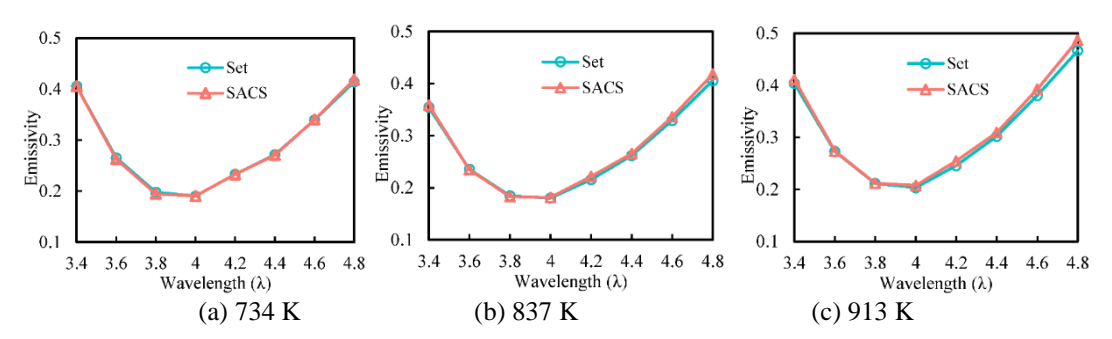


Figure 4 Emissivity inversion results of different materials with different true temperature.

Tab. 4 shows that the largest average absolute error is 2.16 K, the largest average relative error is 0.24 %. These values depict the algorithm's precision in capturing temperature inversion, showcasing its ability to deliver consistently accurate results even under varying thermal conditions. Furthermore, by demonstrating the alignment of the calculated emissivity trends with the true distribution for zirconia samples, Fig. 4 emphasizes the algorithm's capability to effectively discern and approximate material-specific thermal responses across different wavelength ranges. The findings presented in Table 4 and Figure 4 collectively affirm the utility and reliability of the SACS algorithm in the domain of multispectral thermometry. Given the algorithm's consistent accuracy in temperature inversion and its adeptness at approximating material emissivity, it emerges as a robust and dependable data processing method for extracting valuable thermal information from multispectral data.

These results not only underscore the algorithm's practical applicability but also position it as a crucial tool for industries reliant on precise thermal measurements, thereby contributing to advancements in material science, industrial processes, and environmental monitoring. Therefore, the SACS algorithm can be used as a data processing method for multispectral thermometry.

Illustrated in Figure 5, the comparative analysis aims to provide a direct representation of the SACS algorithm's performance. By evaluating the relative errors between the simulation results and the true values, the study offers a comprehensive insight into the efficacy of the SACS algorithm in contrast to the CS algorithm and the GIM-EPF, IPF, and GP algorithms as outlined in reference [20]. This comparative assessment takes place within the same simulation environment, ensuring a consistent benchmark for evaluation. The results of this comparative evaluation serve to elucidate the distinct operational strengths and limitations of each algorithm, shedding light on their respective abilities to accurately calculate and represent values within a given context. This comparative framework not only highlights the SACS algorithm's individual performance but also enables a holistic understanding of its competitive positioning against well-established alternative algorithms. Additionally, this comparative analysis carries significant implications for the practical deployment of these algorithms, offering valuable insights into their reliability and accuracy in diverse scenarios. As such, these findings are instrumental in informing decisions regarding the selection and implementation of algorithms for real-world applications across various domains, including multispectral thermometry and industrial sensing.

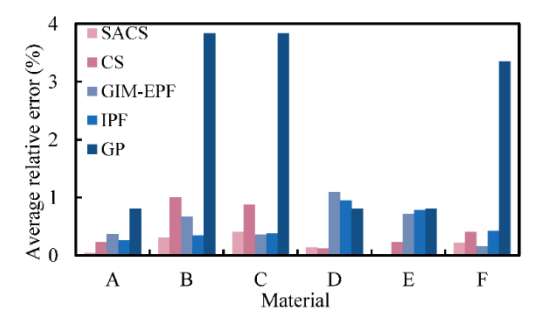
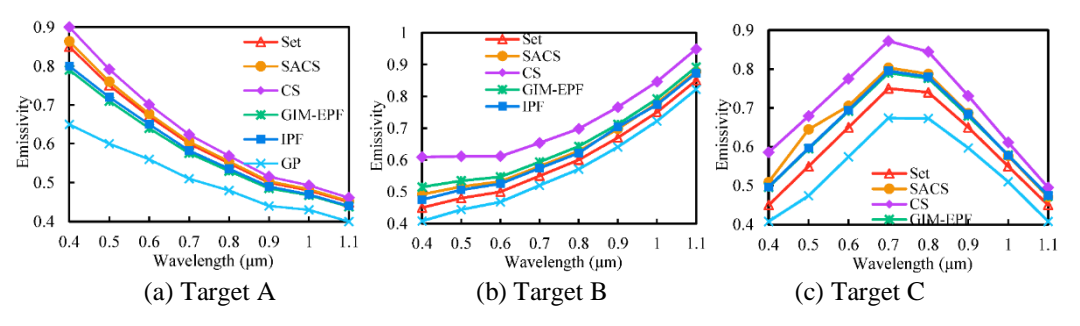


Figure 5 Comparison of the average relative error among SACS algorithm, CS algorithm and other algorithms

Figure 5 demonstrates the remarkable superiority of the SACS algorithm in achieving inversion temperature accuracy compared to alternative algorithms. Notably, the CS algorithm exhibits higher inversion temperature accuracy for specific materials (A, D, E, and F) when compared to the GIM-EPF, IPF, and GP algorithms. These findings underscore the nuanced performance variations of different algorithms across distinct materials, shedding light on their comparative strengths and weaknesses in practical applications. Furthermore, Figure 6 provides valuable insight into the relationship between emissivity curves and wavelength, offering a comparative analysis of the SACS algorithm, CS algorithm, and other algorithms. This visual representation serves to elucidate how these algorithms handle the intricate interplay between emissivity curves and wavelength, providing a deeper understanding of their respective capabilities and limitations in multispectral thermometry. Understanding these distinctions is crucial for effectively leveraging these algorithms in industrial settings, facilitating informed decision-making regarding their deployment based on the specific material and spectral characteristics encountered. Additionally, these visual representations offer a foundation for further research and development, guiding the refinement and optimization of algorithms to address specific industrial requirements and challenges.



ISSN: 1750-9548

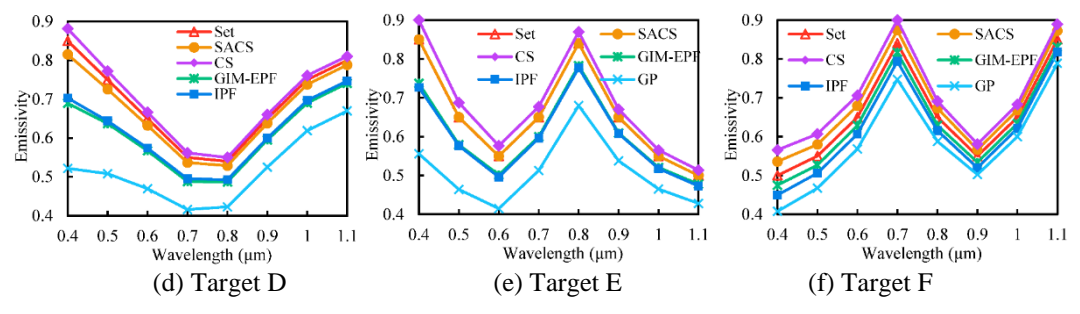


Figure 6 Comparison of the SACS and CS algorithms with other algorithms for inversion emissivity

The SACS algorithm exhibits superior emissivity inversion accuracy across six different materials when compared to other algorithms. This heightened precision underlines the algorithm's efficacy in reliably estimating emissivity, a critical factor in temperature measurement. Moreover, the SACS algorithm's average computational speed surpasses that of the CS algorithm by almost sixfold and exceeds the GIM-EPF algorithm by a staggering 12-fold. This remarkable performance in computation time highlights the SACS algorithm's efficiency. Beyond its speed and accuracy, the SACS algorithm's practicality and suitability for industrial applications are noteworthy. With its rapid calculation time, minimal temperature errors, and consistent performance, the algorithm emerges as an optimal choice for real-time temperature monitoring in hightemperature industrial settings. Its stable and reliable nature positions it as a key tool for ensuring precision and efficiency in industrial processes, thereby contributing to enhanced productivity and safety. Looking ahead, further exploration into the algorithm's adaptability to diverse industrial environments, materials, and noise levels could solidify its applicability across a broader spectrum of industrial settings. Additionally, ongoing research efforts may focus on integrating machine learning techniques to continually refine and optimize the SACS algorithm, ultimately enhancing its robustness and versatility. In conclusion, the SACS algorithm not only outperforms its counterparts in accuracy and speed but also holds immense promise for practical implementation in multispectral thermometry. Its advantages in speed, accuracy, and stability position it as a pivotal tool for precise and efficient temperature measurement, with potential far-reaching impacts across various industrial sectors.

6. Conclusions

In an effort to address the challenges inherent in multispectral thermometry, including issues with excessively broad emissivity search ranges, uncertain initial solutions, and prolonged computation times, a novel data processing model for multispectral thermometry has been devised. This model involves a redefinition of the objective function and constraint conditions. Additionally, a self-adaptive cuckoo algorithm has been introduced to enhance the process. The effectiveness of this self-adaptive cuckoo algorithm has been substantiated through the inversion calculation of six distinct emissivity models utilizing zirconia samples. The maximum relative error of the self-adaptive cuckoo algorithm is 0.41% in scenarios without noise interference and 0.91% in cases with noise interference. Notably, the self-adaptive cuckoo algorithm demonstrates robust temperature inversion capabilities even under low signal-to-noise ratios, with experimental results highlighting temperature inversion errors below 0.25%. This approach introduces a new perspective to the field of multispectral temperature measurement. Moreover, the SACS algorithm's computation time is a mere 0.34 seconds, making it nearly six times faster than the CS algorithm and twelve times faster than the GIM-EPF algorithm on average. In conclusion, the SACS algorithm offers precise and efficient temperature estimation and holds potential for application in real-time high-temperature industrial measurements. The significance of this research in advancing multispectral thermometry lies in its capacity to address critical challenges faced in hightemperature industrial settings. By introducing the SACS algorithm, this study has significantly improved the accuracy and efficiency of temperature estimation, crucial for real-time monitoring and control of industrial processes operating at elevated temperatures. However, certain limitations and areas for future development should be carefully considered. While the SACS algorithm demonstrates impressive performance, further validation across diverse industrial environments and material compositions could enhance its robustness and reliability. Additionally, the potential impact of varying surface conditions and complex emissivity spectra on

the algorithm's accuracy should be thoroughly investigated to ensure its versatility. Enhancing its adaptability to varying noise levels and expanding its use to encompass different material types will be essential for its widespread adoption. In conclusion, the development and application of the SACS algorithm represent a significant advancement in multispectral thermometry, offering precise and efficient temperature estimation with promising potential for real-time industrial measurements in high-temperature environments. By addressing the current limitations and continuing to refine its capabilities, the SACS algorithm stands to make a meaningful impact in industrial temperature monitoring and control, enhancing process efficiency and safety across a wide range of industrial sectors.

Acknowledgements

This study is supported by Defence Industrial Technology Development Program and the central government guides local science and technology development foundation and the Natural Science Foundation of Hebei Province, China.

References

- [1] Ladaci A, Cheymol G, Maskrot H, Gonnier C. Measurement of reactor core temperature using multispectral infrared pyrometry in accidental conditions. The European Physical Journal Conferences. 2020, 225(9): 1-2.
- [2] Mekhrengin MV, Meshkovskii IK, Tashkinov VA, Guryev VI, Sukhinets AV, et al. Multispectral pyrometer for high temperature measurements inside combustion chamber of gas turbine engines. Measurement. 2019, 139: 355–360.
- [3] Urban JL, Vicariotto M, Dunn-Rankin D, Fernandez-Pello AC. Temperature measurement of glowing embers with color pyrometry. Fire Technology. 2019, 55: 1013–1026.
- [4] Akbarnozari A, Ben-Ettouil F, Amiri S, Bamber O, Grenon JD, et al. Online diagnostic system to monitor temperature of in-flight particles in suspension plasma spray. Journal of Thermal Spray Technology. 2020, 29: 908–920.
- [5] Szulc M, Kirner S, Forster G, Schein J. A novel approach to determine in-flight particle oxidation for thermal spraying processes. Journal of Thermal Spray Technology. 2020, 29: 932–946.
- [6] Coates PB. The least-square approach to multi-wavelength pyrometry. High Temperatures. 1988, 20: 433–441.
- [7] Araújo A. Analysis of multiband pyrometry for emissivity and temperature measurements of gray surfaces at ambient temperature. Infrared Physics and Technology. 2016, 76: 365–374.
- [8] Cui S, Xing J, Jian Xing. Research on calibration method of infrared temperature measurement system near room temperature field. Frontiers in Physics. 2022, 9: 786443.
- [9] Wen CD, Mudawar I. Experimental investigation of emissivity of aluminumalloys and temperature determination using multispectral radiation thermometry (MRT)algorithms. Journal of Materials Engineering Performance. 2002, 11(5): 551–562.
- [10] Wen CD. Investigation of steel emissivity behaviors: Examination of Multispectral Radiation Thermometry (MRT) emissivity models. International Journal of Heat and Mass Transfer. 2010, 53(9–10): 2035–2043.
- [11] Wen CD, Mudawar I.. Mathematical determination of emissivity and surface temperature of aluminum alloys using multispectral radiation thermometry. International communications in heat and mass transfer. 2006, 33(9): 1063–1070.
- [12] Sun XG. Research on the Data Processing Method of Solid Propellant Rocket Engine Plume Temperature. Journal of Infrared and Millimeter Waves. 2003, 22(2): 141–144.
- [13] Sun XG, Yuan GB, Dai JM, Chu Z.X.. Processing method of multi-wavelength pyrometer data for continuous temperature measurements. International Journal of Thermophysics. 2005, 26(4): 1255–1261.
- [14] Dai J. Research on Genetic Algorithm for Plume Temperature of Solid Propellant Rocket Engine. Journal of Combustion Science Technology. 2006, 12(3): 213–216.
- [15] Xing J, Peng B, Ma Z, Gao X, Dai L, et al. Directly data processing algorithm for multiwavelength pyrometer (MWP). Optics Express. 2017, 25(24): 30560–30574.
- [16] Liang J, Dai L, Chen S, Gu W, Peng B, et al. Generalized inverse matrix-exterior penalty function (GIM-EPF) algorithm for data processing of multi-wavelength pyrometer (MWP). Optics Express. 2018, 26(20): 25706.
- [17] Zhang Y, Zou Z, Yan F. A multispectral thermometry based on multi-objective constraint optimization. Measurement. 2022, 192: 110813.

International Journal of Multiphysics

Volume 18, No. 3, 2024

ISSN: 1750-9548

- [18] Tian Z, Zhang K, Xu Y, Yu K, Liu Y. Data processing method for simultaneous estimation of temperature and emissivity in multispectral thermometry. Optics express. 2022, 30(20): 35381-35397.
- [19] Kun Y, Huige G, Kaihua Z, Liu Y. Multi-wavelength radiometric thermometry data processing algorithm based on the BFGS algorithm. Applied optics. 2021, 60(7): 1916-1923.
- [20] Liang J, Dai L, Chen S, Gu W, Peng B, et al. Generalized inverse matrix-exterior penalty function (GIM-EPF) algorithm for data processing of multi-wavelength pyrometer (MWP). Optics express. 2018, 26(20): 25706-25720.